Quantum Dynamics and Spectroscopy of Electron Photodetachment in Cl⁻···H₂O and Cl⁻···D₂O Complexes

Martina Roeselová,[†] **Martin Mucha,**[†] **Burkhard Schmidt,**[‡] **and Pavel Jungwirth*,**[†]

J. Heyrovský Institute of Physical Chemistry, Academy of Sciences of Czech Republic and Center for Complex Molecular Systems and Biomolecules, Dolejškova 3, 18223 Prague, Czech Republic, and Institut für Mathematik, Scientific Computing, Freie Universität Berlin, Arnimallee 2-6, 14195 Berlin, Germany

We have modeled electron photodetachment spectra of Cl⁻···H₂O and Cl⁻···D₂O complexes using 3D quantum dynamical simulations on the three low-lying electronic states of the nascent neutral systems. Time-dependent quantum simulations combined with anionic and neutral stationary-state calculations by imaginary time propagation allowed for a detailed interpretation of the spectral features in terms of the underlying dynamics. Because of large differences between the anionic and neutral potential surfaces, the systems are found after electron photodetachment primarily high above the dissociation threshold. Nevertheless, pronounced long-lived resonances are observed, particularly for the lowest neutral state, reflecting the fact that a significant portion of the excess energy is initially deposited into nondissociative modes, that is, to (hindered) water rotation. These resonances form bands corresponding to water rotational states with a fine structure due to intermolecular stretch progressions. Comparison is made to experimental zero electron kinetic energy (ZEKE) spectra of the I⁻···H₂O complex, where analogous anharmonic vibrational progressions have been observed.

1. Introduction

The anion zero electron kinetic energy (ZEKE) spectroscopy[1−4] represents a unique tool for studying structure and dynamics of size-selected neutral molecular clusters. The basic idea is to perform size selection via mass spectrometry of anionic precursors and, subsequently, photodetach the electron. Because of the relatively high resolution of the ZEKE method ($\sim$1 cm⁻¹), rovibrational states of the nascent neutral complex can be probed. Because electron photodetachment is a vertical process and optimal geometries of the anion and corresponding neutral clusters can differ significantly, the ZEKE spectra are often very complex and their assignment is by no means trivial. Provided that the nascent neutral complex is an open-shell species (radical), the situation can be further complicated by the existence of low-lying excited electronic states. Quantitative computational modeling of the spectra can then become an important ingredient for correct interpretation of the experimental data in terms of the underlying quantum dynamics.

Faithful simulation of spectra requires, in addition to high-quality potential energy surfaces, an accurate quantum mechanical description of the nuclear degrees of freedom. Traditionally, spectra are modeled within a time-independent framework by evaluation of all of the individual Franck−Condon overlaps.[5] However, in certain cases, for example, when the spectrum is dominated by short-lived dissociative states or finite lifetime resonances, it can be computationally more advantageous to work in the time-dependent framework.[6] Within this approach, the initial wave function, which is a stationary (e.g., ground) state on the anionic potential, is allowed to evolve in time on the potential of the neutral complex. The spectrum is then obtained as a Fourier transform of the autocorrelation function, which is the time-dependent overlap of the evolving wave function with the initial wave function.[7,8] In principle, one should perform the propagation for infinite time; however, in practice, it suffices to propagate long enough to reach spectral resolution comparable to that of the experiment.

Size-selected halide−water clusters, which represent a natural laboratory for studying the onset of ionic aqueous solvation, have been extensively studied by means of photoelectron spectroscopy,[4,9] as well as via ab initio quantum chemistry methods,[10−14] molecular dynamics (MD),[15−18] and quantum vibrational dynamics[19] simulations. With the advent of ZEKE spectroscopy, the hitherto unexplored neutral complexes, created by electron photodetachment, became also accessible to experimental scrutiny. Several years ago, ZEKE spectra of the I⁻···H₂O complex have been published.[20] The study of the iodide−water complex indicated among others that the dynamics following electron photodetachment is significantly more complicated than that of the halide−rare gas atom clusters, investigated by the ZEKE technique earlier.[21,22] The ZEKE spectra of the halide−rare gas atom systems reflect a simple, one-dimensional motion along the interatomic stretching coordinate on each of the three low-lying potential surfaces. These potentials, which are split by the presence of the rare gas atom and by the spin−orbit interaction, qualitatively correlate with the three possible orientations of the singly occupied p-orbital of the nascent halogen radical. In the case of the I⁻···H₂O cluster, the ZEKE signal is a result of a much more complex, three-dimensional intermolecular nuclear dynamics (internal water vibrational modes can be considered as frozen) on the three low-lying neutral potential surfaces,[20] and a simple interpretation in terms of single mode vibrational progressions is no more possible.

In our previous computational studies[23−25] of halide−water complexes, we have addressed the following issues: First, we

* To whom correspondence should be addressed. E-mail: jungwirt@jh-inst.cas.cz.
 † Academy of Sciences of Czech Republic and Center for Complex Molecular Systems and Biomolecules.
 ‡ Freie Universität Berlin.

have performed extensive ab initio scans of all three low-lying neutral potential energy surfaces of clusters containing chlorine or bromine and a single water molecule. Moreover, we have fitted the neutral surfaces to a diatomics-in-molecule potential model,[26-28] suitable for subsequent dynamical studies. Second, we have modeled the electron photodetachment process in these two systems by means of quasi-classical MD, that is, running a swarm of Wigner trajectories on the lowest neutral surface. As a principal result, we have found that the complexes practically do not directly dissociate even though upon electron photodetachment the neutral clusters are born above the dissociation threshold. This is because most of the excess energy is initially deposited into the internal water rotation. Only later, the energy is transferred also to the intermolecular stretching mode, which eventually leads to dissociation into a halogen radical and water molecule. This dynamical evolution is a direct consequence of large differences in the shapes of the anionic and neutral potential energy surfaces. While the anion is strongly hydrogen-bonded, the neutral system prefers geometries with water hydrogens pointing away from the halide.

The principal goal of the present study is to proceed to quantitative photoelectron spectra modeling of $Cl^-\cdots H_2O$ and $Cl^-\cdots D_2O$ complexes by performing wave function propagations for the three intermolecular nuclear degrees of freedom and on the three low-lying adiabatic neutral potential surfaces in a numerically exact way. In addition, we also perform stationary calculations of a set of vibrational states of both anionic and neutral complexes. This combined time-dependent and time-independent approach then allows us not only to predict the photoelectron spectra but also to interpret in detail the spectral features in terms of underlying nuclear dynamics.

The rest of the paper is organized as follows. Section 2 describes the anionic and neutral systems and the corresponding interatomic interactions. Section 3 deals with the details of the quantum dynamical calculations in real, as well as in imaginary, time. Bound vibrational states of the anionic and neutral clusters are discussed in section 4, while the results of real-time propagations and the simulated ZEKE spectra are presented in section 5. Finally, section 6 contains a brief summary.

2. Systems and Interactions

For the purpose of the present study, we treat the H_2O molecule as a rigid body (O—H bonds frozen at 0.96 Å and H—O—H angle fixed at 104°). Furthermore, in accordance with the cryogenic experimental conditions, we assume that before electron photodetachment the complex is in its ground vibrational and rotational state. As far as the overall rotation of the complex is concerned, this is certainly an approximation. However, it can be justified by the fact that for low-lying rotational states, which can be populated in the experiment, the vibrational—rotational coupling is negligible. Because of conservation of total angular momentum, the condition of zero overall rotation has to be fulfilled throughout the whole simulation. Thus, the problem reduces to three dimensions corresponding to the intermolecular degrees of freedom, for the description of which we adopt the generalized Jacobi coordinates[29,30] shown in Figure 1. The length of the vector from the center of mass of the water molecule to the halogen atom is denoted R, θ is the angle between R and the C_2 axis of water ($\theta = 0°$ corresponds to the Cl atom on the C_2 axis and facing the H atoms), and ϕ is the angle of rotation about the C_2 axis (with $\phi = 0°$ corresponding to the planar geometry of the complex).

2.1. Anionic Complex. The anionic $Cl^-\cdots H_2O$ complex represents a precursor from which dynamics is initiated by
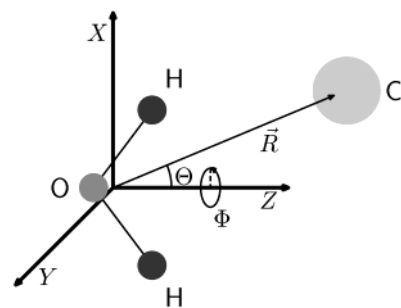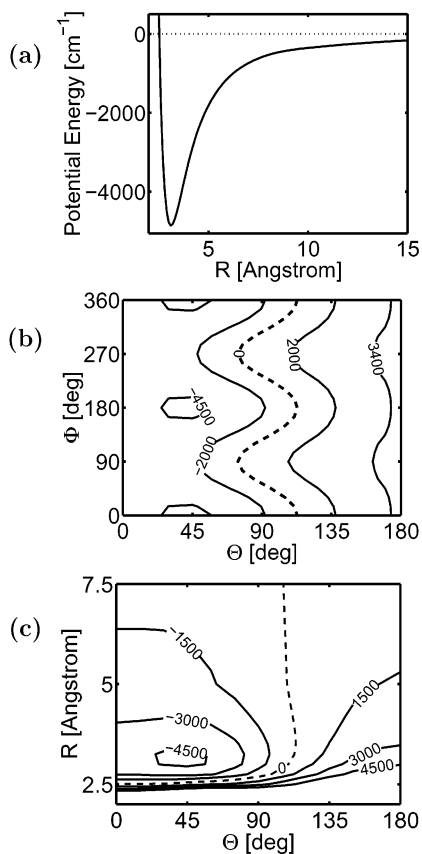

Figure 1. Definition of Jacobi coordinates.
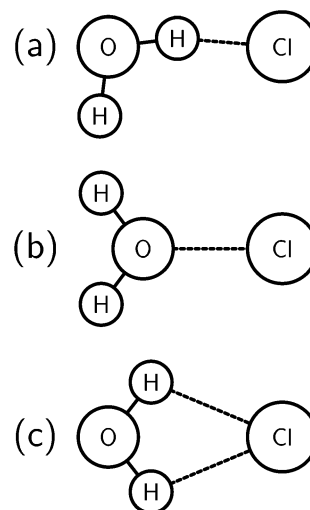
Figure 2. Optimal structures of (a) the anionic $Cl^-\cdots H_2O$ complex and (b) the neutral $Cl^\bullet\cdots H_2O$ complex and (c) C_{2v} symmetric geometry with the Cl atom on the C_2 axis and facing the hydrogens.

electron photodetachment. To calculate the bound rovibrational states of the anionic complex by solving numerically exactly the three-dimensional Schrödinger equation, we have first performed a systematic scan of the potential energy surface of the ground electronic state of the anionic $Cl^-\cdots H_2O$ complex. A total of ∼1700 points on the PES have been calculated for R between 2 and 30 Å, for the full range of the in-plane angular coordinate, $\theta \in (0°, 180°)$, and for the first quadrant of the out-of-plane angular coordinate, $\phi \in (0°, 90°)$. The PES for the remaining three quadrants has been then constructed exploiting the symmetry properties of the C_{2v} point group. The calculation has been carried out applying the coupled cluster method with single and double excitations, and including triple excitations perturbatively (CCSD(T))[31] with the augmented correlation-consistent polarized valence double-ζ basis set (aug-cc-pVDZ)[32,33] using the Gaussian 98 program package.[34]

The resulting potential has a global minimum of -4854 cm^{-1} (with respect to dissociation into Cl^- and H_2O fragments) at $R = 3.15$ Å, corresponding to a planar geometry of the complex ($\phi = 0°$ or $\phi = 180°$) with a nearly collinear Cl^-—H—O hydrogen bond ($\theta = 44°$). This structure (see Figure 2a) is in a quantitative agreement with previous calculations,[10-12,14,25] as well as experimental studies,[35,36] given the geometry constraint of the rigid water molecule mentioned above. The asymmetric, hydrogen-bonded optimal structure is preferred within a rather narrow region of R values around 3 Å. At shorter radial separations ($R \approx 2.5$ Å), the repulsive forces begin to repel the hydrogen atom away from the almost linear hydrogen-bonded arrangement. In this short-range region, as well as at larger radial distances ($R > 5$ Å), the symmetric C_{2v} geometry ($\theta = 0°$, independent of ϕ) with the Cl atom on the C_2 axis and

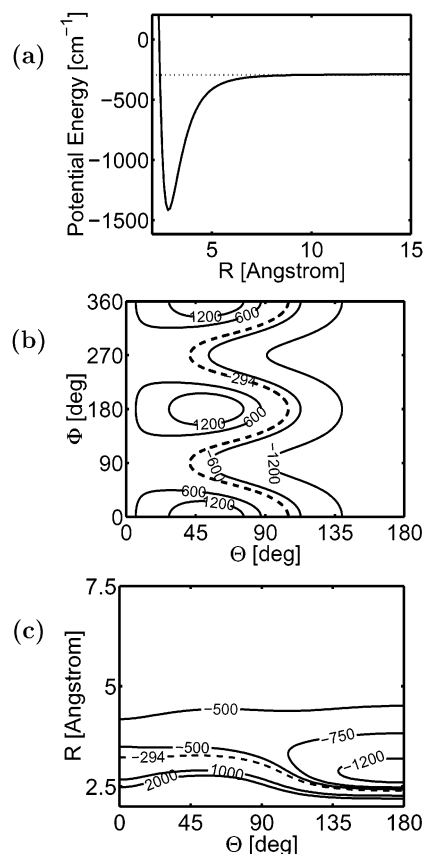Electron Photodetachment in Cl⁻···H₂O and Cl⁻···D₂O

J. Phys. Chem. A, Vol. 106, No. 51, 2002 **12231**

Figure 3. Ground-state potential energy surface of anionic Cl⁻···H₂O complex: (a) radial dependence for optimal orientation of water molecule ($\theta = 44°$, $\phi = 0°$); (b) angular contour plot for $R = 3.25$ Å (close to the optimal radial separation); (c) in-plane radial−angular contour plot for $\phi = 0°$. Energy scale of the contour plots is in cm⁻¹; dissociation threshold $E = 0$ cm⁻¹ is denoted by dashed line.
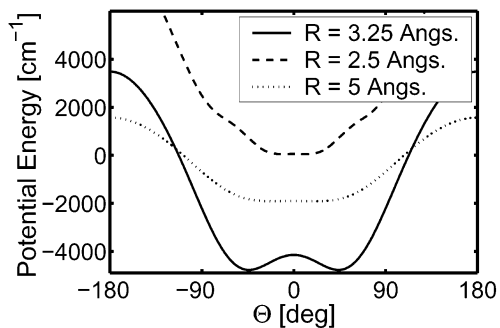
Figure 4. Ground-state potential energy surface of anionic Cl⁻···H₂O complex along the tunneling coordinate θ for three different radial separations: $R = 2.5$ Å (dashed line); $R = 3.25$ Å (full line); $R = 5.0$ Å (dotted line).

facing the hydrogens (see Figure 2c) has the lowest energy. In the hydrogen-bonding region of R around 3 Å, this C_{2v} structure corresponds to a transition state separating the two equivalent minima between which the system can tunnel. The height of the tunneling barrier is 750 cm⁻¹ at the optimal distance of $R = 3.15$ Å. The situation is illustrated in Figures 3 and 4. Figure 3a shows the radial dependence of the Cl⁻···H₂O potential for optimal values of the angular coordinates ($\phi = 0°$, $\theta = 44°$). Figure 3b depicts the angular contour plot of this potential for $R = 3.25$ Å. In Figure 3c, in-plane radial−angular contour plot (for $\phi = 0°$) is presented. Finally, the potential along the "tunneling coordinate" θ for three selected values of R is depicted in Figure 4.

Figure 5. Ground-state potential energy surface of neutral Cl•···H₂O complex: (a) radial dependence for optimal orientation of water molecule ($\theta = 180°$, $\phi = 0°$); (b) angular contour plot for the optimal radial separation of $R = 2.8$ Å; (c) in-plane radial−angular contour plot for $\phi = 0°$. Energy scale of the contour plots is in cm⁻¹; dissociation threshold of −294 cm⁻¹ is depicted by dashed line.

2.2. Neutral Complex. In this study, we investigate the electronically adiabatic quantum nuclear dynamics following electron photodetachment in Cl⁻···H₂O cluster. We take into account the three lowest electronic states of the neutral Cl•···H₂O complex, corresponding to different orbital orientations of the unpaired p-electron of the chlorine radical. A detailed description of the potential model, which combines a thorough ab initio scan with a diatomics-in-molecule fit (DIM) including the effect of the spin−orbit interaction, has been reported in our previous work.[23−25] Here, we want to focus on those features of the lowest three adiabatic neutral potential energy surfaces that are important for understanding the photodetachment spectra. Note that the spin−orbit term splits the common dissociation threshold of the three potentials by lowering the dissociation energy of the ground ($X_{1/2}$) and the first excited ($I_{3/2}$) states by $^1/_3\Delta$ to −294 cm⁻¹, while the dissociation energy of the second excited state ($II_{1/2}$) increases by $^2/_3\Delta$ to +588 cm⁻¹ ($\Delta = 882.4$ cm⁻¹ is the spin−orbit constant of the chlorine radical).

Compared to its anionic precursor, the neutral Cl•···H₂O complex is much more weakly bound. The potential energy surface of the ground electronic state has a global minimum of a relative well depth of −1121 cm⁻¹ at $R = 2.8$ Å (see Figure 5a) with oxygen pointing toward chlorine (Figure 2b). Such an equilibrium structure can be rationalized in terms of the (halogen) quadrupole−(water) dipole electrostatic interaction, which together with dispersion constitutes the dominant contributions to the halogen−water intermolecular potential in the neutral complex. The preference for this arrangement is illustrated by Figure 5b, which shows the angular contour plot

of the neutral ground-state potential for the optimal radial distance of $R = 2.8$ Å, as well as by Figure 5c in which the in-plane radial–angular contour plot (for $\phi = 0°$) is depicted. Thus, there is a significant difference between the optimal structures of the anionic and the neutral complexes resulting in a strong torque upon electron photodetachment.

Note that our DIM potential does not support another isomer such as the very shallow minimum close to the anionic geometry calculated recently.[14] The corresponding structure at $R = 3.55$ Å is within our potential model a first-order saddle point with respect to the out-of-plane motion of the water molecule. As will be discussed later, however, possible existence of such a shallow local minimum does not play any significant role in the dynamics following electron photodetachment.

Unlike the ground state, the upper two electronic states are mostly repulsive with only shallow minima: $\Delta E_{min} = -153$ cm^{-1} at $R = 3.7$ Å for the first excited state, and $\Delta E_{min} = -283$ cm^{-1} at $R = 3.6$ Å for the second excited state. In both cases, the structure of the complex with the two hydrogens pointing away from chlorine is again energetically most favorable, that is, the angular character of the lowest three neutral electronic states is similar. The strong dependence of the neutral potentials on the mutual orientation of the water molecule and the chlorine radical indicates a possibility of a nonnegligible coupling between angular and radial degrees of freedom. This fact and the significant difference between the optimal structures of the anionic and the neutral complexes are the key factors that make the usual interpretation of the photodetachment process based on one-dimensional (R-dependent only) cuts through anionic and neutral potential energy surfaces invalid.

3. Quantum Dynamics

3.1. Representation. Dynamical simulations, as well as bound-state calculations, have been performed within the Born–Oppenheimer approximation using a coupled channel scheme with an exact form of the Hamiltonian for an atom–(rigid) triatom system expressed in generalized Jacobi coordinates (see Figure 1),

$$\hat{H} = -\frac{\hbar^2}{2\mu R}\frac{\partial^2}{\partial R^2}R + \frac{\hat{l}^2}{2\mu R^2} + \hat{H}^w + V(R,\theta,\phi) \quad (1)$$

where $\mu = m_{H_2O}m_{Cl}/(m_{H_2O} + m_{Cl})$ is the reduced mass of the complex and $\hat{l}$ is the angular momentum operator for end-over-end rotation of the complex. $\hat{H}^w$ is the asymmetric rotor Hamiltonian corresponding to the (internal) water rotation, expressed in terms of the angular momentum operator $\hat{j}$ and its components $\hat{j}_x$, $\hat{j}_y$, $\hat{j}_z$, and "ladder" operators $\hat{j}_+ = \hat{j}_x + i\hat{j}_y$, $\hat{j}_- = \hat{j}_x - i\hat{j}_y$,

$$\hat{H}^w = A\hat{j}_x^2 + C\hat{j}_y^2 + B\hat{j}_z^2 = \alpha\hat{j}^2 + \beta\hat{j}_z^2 + \gamma(\hat{j}_+^2 + \hat{j}_-^2) \quad (2)$$

In accordance with ref 29, we use a coordinate system with the origin at the center of mass of the water molecule and the x, y, and z axes oriented along the H_2O A, C, and B axes, respectively. Coefficients α, β, and γ in eq 2 are then defined as the following linear combinations of water rotational constants A, B, and C:

$$\alpha = \frac{1}{2}(A + C), \quad \beta = B - \frac{1}{2}(A + C), \quad \gamma = \frac{1}{4}(A - C) \quad (3)$$

The values of rotational constants of the H_2O molecule, $A = 27.88$, $B = 14.51$, and $C = 9.28$ cm^{-1}, have been taken from ref 29; those of D_2O, $A = 15.42$, $B = 7.27$, and $C = 4.85$ cm^{-1}, have been taken from ref 5. Finally, $V(R,\theta,\phi)$ in eq 1 is the

intermolecular potential for interaction of water molecule either with chloride ion in the anionic complex or with chlorine radical in one of the lowest three adiabatic electronic states of the neutral complex. In either case, the interaction potential $V(R,\theta,\phi)$ reflects the C_{2v} symmetry of the water molecule. The generalized Jacobi coordinates R, θ, and ϕ correspond to the spherical polar coordinates of chlorine with respect to the above-defined water-centered x, y, z frame.

In this study, we have assumed that the total angular momentum $\hat{J} = \hat{l} + \hat{j}$ is equal to zero. This leads to a significant reduction of the number of coupled states that have to be included in the coupled channel scheme, because then $\hat{l}^2 = \hat{j}^2$. It also allows us to perform all of the calculations in the water-fixed coordinate system rather than in the complex-fixed frame attached to the halogen–water complex as a whole, as it would be inevitable in the general case of $\hat{J} \neq 0$.[29,37] The total nuclear wave function can be then expanded in C_{2v} symmetry-adapted spherical harmonics (SASHs), $Y_{jk}^{(S)}(\theta,\phi)$,

$$\Psi(R,\theta,\phi,t) = \frac{1}{R}\sum_{jk}\chi_{jk}^{(S)}(R,t)Y_{jk}^{(S)}(\theta,\phi) \quad (4)$$

The $Y_{jk}^{(S)}(\theta,\phi)$ SASHs are obtained as linear combinations of spherical harmonics $Y_{jk}(\theta,\phi)$,

$$Y_{jk}^{(S)}(\theta,\phi) \approx \frac{1}{\sqrt{2}}(Y_{jk}(\theta,\phi) \pm Y_{j-k}(\theta,\phi)) \quad (5)$$

where k is a projection along the $z \equiv B$ axis.[38] Symmetry-adapted $Y_{jk}^{(S)}(\theta,\phi)$ functions (as well as the $Y_{jk}(\theta,\phi)$ ones) are eigenfunctions of the water angular momentum operator $\hat{j}^2$ and represent here the channel functions describing the angular motions corresponding to the internal rotation of water molecule. Substitution of the expansion given in eq 4 into the Schrödinger equation with the Hamiltonian given by eq 1 yields a set of coupled equations for the radial functions $\chi_{jk}^{(S)}(R,t)$:

$$i\hbar\frac{\partial}{\partial t}\chi_{jk}^{(S)}(R,t) = \left(-\frac{\hbar^2}{2\mu}\frac{\partial^2}{\partial R^2} + \frac{\hbar^2 j(j+1)}{2\mu R^2}\right)\chi_{jk}^{(S)}(R,t) + \sum_{j'k'}(H_{jkj'k'}^w + V_{jkj'k'}(R))\chi_{j'k'}^{(S)}(R,t) \quad (6)$$

where the last term on the right-hand side, comprising the asymmetric rotor Hamiltonian matrix and the potential matrix, is responsible for the couplings between the individual channels. The matrix representation of the asymmetric rotor Hamiltonian $\hat{H}^w$ can be readily obtained in the basis of spherical harmonics $Y_{jk}(\theta,\phi)$, where the matrix elements are given by

$$H_{jkj'k'}^w = \hbar^2(\alpha j(j+1) + \beta k^2)\delta_{jj'}\delta_{kk'} + \gamma\hbar^2\sqrt{(j+1+k)(j-k)(j+2+k)(j-1-k)}\delta_{jj'}\delta_{k',k+2} + \gamma\hbar^2\sqrt{(j+k)(j+1-k)(j-1+k)(j+2-k)}\delta_{jj'}\delta_{k',k-2} \quad (7)$$

and subsequently transformed into the symmetry-adapted basis $Y_{jk}^{(S)}(\theta,\phi)$. This transformation leads to the factorization of the $\hat{H}^w$ matrix into four blocks, each corresponding to one irreducible representation of the C_{2v} point group.[39] To obtain the matrix elements of the potential

$$V_{jkj'k'}(R) = \int\sin\theta\,d\theta\int d\phi\,Y_{j'k'}^{(S)}(\theta,\phi)V(R,\theta,\phi)Y_{jk}^{(S)}(\theta,\phi) \quad (8)$$

Electron Photodetachment in Cl⁻···H₂O and Cl⁻···D₂O

J. Phys. Chem. A, Vol. 106, No. 51, 2002 **12233**

the integrals over the surface of a unit sphere were calculated employing the Gauss–Legendre quadrature.[40] For anionic, as well as neutral, potentials, 151 points in both cos θ and ϕ were sufficient to obtain converged results. Because the potential function $V(R,\theta,\phi)$ transforms according to the totally symmetric irreducible representation A_1 of the C_{2v} point group, the potential matrix has the same block structure as the above $\hat{H}^w$ matrix.

3.2. Bound-State Calculations. For the purpose of simulating the photodetachment dynamics under cryogenic conditions, we are primarily interested in calculating the ground state of the anionic complex, which represents the initial state in the process under study. However, for the sake of completeness, we have also calculated energies and wave functions of low-lying excited rovibrational states of the anionic Cl⁻···H₂O complex, as well as those of the lowest three electronic states of its neutral Cl•···H₂O counterpart. Stationary states were calculated by the method of imaginary time propagation.[41] Using this technique, one solves the eigenvalue problem by formally solving the time-dependent Schrödinger equation (i.e., eq 6) in which one substitutes $t \leftarrow i\tau$. One first finds the ground state Ψ_0 on a given potential $V(R,\theta,\phi)$ by applying the evolution operator $\hat{U} = e^{-\hat{H}\tau}$ onto an arbitrary initial guess function $\Psi(\tau=0)$ (having a non-zero overlap with Ψ_0) and propagating for sufficiently long imaginary time τ. Higher states Ψ_i can then be obtained sequentially by projecting out all of the lower states $\Psi_0, ..., \Psi_{i-1}$ from the initial guess wave function $\Psi(\tau=0)$ before applying the evolution operator. This method is found to be stable for at least a few tens of bound states. It also serves to identify several long-lived resonances. Expansion of the imaginary time evolution operator in terms of Chebyshev polynomials[41–43] with (imaginary) time step of 35 fs has been used to perform the actual propagation. Typically, the number of Chebyshev polynomials in the expansion was within the range of 60–80. Tens to hundreds of steps were needed to obtain converged results. Radial coefficients $\chi_{jk}^{(S)}(R,t)$ (see eq 4) were represented on an equidistant R grid of 512 points between 2 and 30 Å. A total of 72, 64, 56, and 72 angular basis functions (corresponding to $j_{max} = 15$) have been used to calculate the A_1, B_1, A_2, and B_2 states, respectively.

3.3. Simulation of Spectra. A common approach toward spectra is to consider them as a time-independent property, characteristic for a given species. However, the transitions that give rise to spectra involve motions of electrons and nuclei within the system under study. As has been first shown by Heller,[7,8] description of the underlying dynamics thus provides an alternative, time-dependent approach to spectroscopy.

Simulation of the dynamics following the electron photodetachment in Cl⁻···H₂O complex starts with the anionic system in a stationary state. Because of cryogenic experimental conditions, we assume that the anionic complex prior to photodetachment is in its electronic, vibrational, and rotational ground state, Ψ_0. At time $t = 0$, the photodetachment accompanied by an electronic transition takes place. In terms of potential energy surfaces, this process can be viewed as vertical promotion of the initial wave function Ψ_0 from the anionic PES onto any of the three adiabatic electronic PESs of the neutral system. Here, the initial wave packet Ψ_0 is no longer stationary but rather evolves in time according to the time-dependent Schrödinger equation. Thus, our methodology is analogous to the time-dependent approach to photodissociation.[37] The corresponding Hamiltonian is given by eq 1, where $V(R,\theta,\phi)$ represents one of the three neutral electronic potential surfaces. Within the Born–Oppenheimer approximation, all nonadiabatic couplings between the different electronic states are neglected, and the
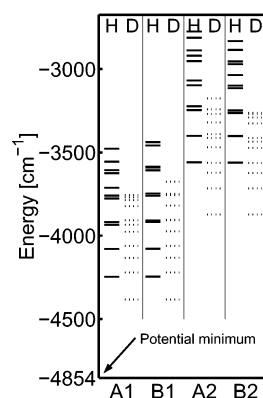
Figure 6. Energy level diagram of lowest rovibrational states of anionic Cl⁻···H₂O (left subcolumns) and Cl⁻···D₂O (right subcolumns) complexes for all irreducible representations of the C_{2v} point group.

initial wave packet is propagated on each surface separately. On the basis of results of our previous nonadiabatic study of a similar system, the Cl–HCl complex,[44] we expect these couplings to be weak.

The spectrum $I(\omega)$ arising from the transition to the corresponding electronic state of the neutral complex is then obtained by evaluating the autocorrelation function, that is, the overlap of the wave function at time t with the initial wave function, and performing the Fourier transform

$$I(\omega) \propto \int_{-\infty}^{\infty} e^{i\omega t} \langle \Psi_0 | \Psi(t) \rangle \, dt \qquad (9)$$

To solve the time-dependent Schrödinger equation, the coupled channel scheme described in detail in section 3.1 has been used with the total wave function $\Psi(R,\theta,\phi,t)$ expanded in a time-independent angular basis, $Y_{jk}^{(S)}(\theta,\phi)$. The time-dependent radial coefficients, $\chi_{jk}^{(S)}(R,t)$ were represented on a grid identical to the case of the bound states calculation (see above). A quadratic negative imaginary potential has been added in the region between 25 and 30 Å to smoothly absorb the outgoing parts of the wave function. A total of 72 basis functions of A_1 symmetry and 64 basis functions of B_1 symmetry (corresponding both to $j_{max} = 15$) have been used. Chebyshev propagator with a time step of 30 fs and, typically, 130–150 polynomials in the expansion has been employed. The system has been propagated for 18 ps. This total propagation time has been chosen to ensure that the frequency resolution of the simulated spectra matches the experimental resolution of 1 cm⁻¹.

4. Results: Bound States

4.1. Anionic Complex. We begin with presenting the ground state, as well as several low-lying vibrationally excited states, of the anionic complex, which have been obtained by imaginary time propagation. The corresponding energy levels are given in Figure 6. The stationary states are divided into four groups, which are labeled according to the corresponding irreducible representations, A_1, B_1, A_2, and B_2, of the C_{2v} symmetry group. Eleven lowest stationary states of each symmetry have been calculated for both the Cl⁻···H₂O complex and its fully deuterated Cl⁻···D₂O analogue.

The ground state of the Cl⁻···H₂O complex (A_1 representation) has the energy of $E_0^{(A_1)} = -4246.70$ cm⁻¹. The first excited state is the lowest one in the B_1 manifold and has the energy $E_0^{(B_1)} = -4246.04$ cm⁻¹. Radial probability density

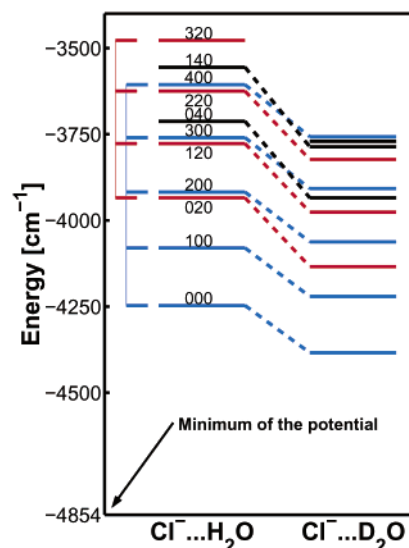$$\rho(R) = R^2 \int_0^{2\pi} \int_0^{\pi} |\Psi(R,\theta,\phi)|^2 \sin\theta \, d\theta \, d\phi \qquad (10)$$
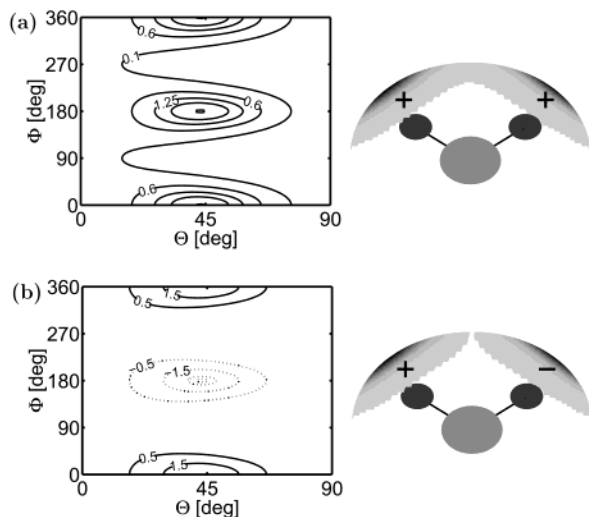
Figure 7. Angular dependence of (a) the ground state (A_1 symmetry) and (b) the first excited state (B_1 symmetry) wave functions of anionic $Cl^-\cdots H_2O$ complex for fixed value of radial coordinate, $R = 3.15$ Å.

Figure 8. Energies of several low-lying states of A_1 symmetry for both $Cl^-\cdots H_2O$ (left subcolumn) and $Cl^-\cdots D_2O$ (right subcolumn) complexes. The states are labeled by three quantum numbers corresponding to the intermolecular stretching, in-plane bending, and out-of-plane bending modes. The stretching vibrational progressions are marked with blue and red colors.

of both of the above states peaks at $R = 3.15$ Å, the optimal chlorine–water distance in the anionic complex. The two wave functions, however, differ in their angular dependence (see Figure 7), the B_1 wave function having a nodal plane coinciding with the $\sigma_v'(yz)$ plane of the water molecule. The near degeneracy of these two states ($\Delta E = 0.66$ cm^{-1}) reflects the tunneling splitting in a double well potential corresponding to the two equivalent $Cl^-\cdots HOH$ geometries (see Figure 4).

The symmetry properties of the above-mentioned lowest two states of the anionic complex have important consequences for the choice of initial conditions for propagation because nuclear spin statistics has to be considered here as well. The two hydrogen nuclei in the water molecule are fermions, and therefore, the overall wave function (vibrational wave function times nuclear spin state) describing the complex should change sign upon their interchange. This implies that only the anionic complex with para-water (antiparallel nuclear spins of the hydrogens) can be found in the A_1 ground state, while the complex with ortho-water (parallel nuclear spins) has to be described by a wave function of the B_1 symmetry. Because of the 1:3 ratio between natural abundances of para- and ortho-water, there is a 75% probability that a given cluster cooled to its lowest accessible state will be described by the B_1 wave function of the first vibrationally excited state rather than by the A_1 ground state. A similar type of arguments applies also to the deuterated $Cl^-\cdots D_2O$ case; however, the ratio between the abundances of the A_1 and B_1 states is now 2:1. We use both the ground state (A_1) and the first excited state (B_1) as the initial condition for propagation on the neutral potentials. The experimental spectra can be then modeled by summing up the two resulting spectra in the appropriate ratio.

Deuteration manifests itself first of all by reduction of the zero-point energy (ZPE), as can be seen directly from Figure 6. Such a reduction in energy results also in more localized vibrational wave functions of the deuterated complex. The influence of deuteration on the frequencies varies according to the way in which the hydrogens are involved in the motion of the individual vibrational modes, that is, on the corresponding reduced masses. Consequently, the effect of deuteration is small for the stretching mode, in which the heavy atoms participate, while it is much larger for the bending mode, in which it is predominantly the two hydrogens that move.

To illustrate the isotope effects in more detail, we present an analysis of the first eleven low-lying states of A_1 symmetry of the anionic complex (see Figure 8). As the three intermolecular modes (chlorine–water stretching vibration, in-plane water bend, and out-of-plane water bend) are well decoupled, it is, at least for the low-lying states presented here, possible to label the energy levels by three quantum numbers. Investigation of the character of the states shown in Figure 8 has revealed a pure vibrational progression corresponding to the intermolecular stretching degree of freedom (states 000, 100, 200, 300, and 400, marked with blue color) with energy spacing of 167, 162, 158, and 154 cm^{-1}, respectively. Angular character of all these states is similar to that of the ground state, and the wave functions differ only by the increasing number of nodes in the radial coordinate. The frequency of the intermolecular stretch, ~160 cm^{-1}, is somewhat smaller than the ab initio harmonic values obtained previously[12,13] at the MP2 level, which are in the range of 187–203 cm^{-1}, and falls within the two reported experimental values of 155[35] and 210 cm^{-1}.[36] Deuteration does not practically affect the vibrational spacing; the energy levels belonging to one stretching vibrational progression merely shift downward as the total ZPE decreases ($\Delta ZPE = 137$ cm^{-1}).

The other states exhibit librational excitation. States 020, 120, 220, and 320 with energy spacing of 158, 152, and 147 cm^{-1} (marked with red color) represent a stretching vibrational progression of the first excited state of the in-plane bend of A_1 symmetry (with two nodes along the θ coordinate). State 040 with four nodes along the θ coordinate corresponds to the second excited state of the in-plane bend within the A_1 manifold. Its angular character is depicted in Figure 9. States 000, 020, and 040 thus form a progression of the in-plane bending libration of the water molecule with spacings of 312 and 222 cm^{-1}. Obviously, unlike the intermolecular stretching, the in-plane bending mode is strongly anharmonic. This finding agrees very well with the recent vibrational self-consistent field calculations.[13] States exhibiting out-of-plane librational excitation belong to the A_2 and B_2 irreducible representations, with the fundamental energy of 687 cm^{-1} (see Figure 6). Upon deuteration, the librational motion is affected significantly more than

Electron Photodetachment in Cl⁻···H₂O and Cl⁻···D₂O

J. Phys. Chem. A, Vol. 106, No. 51, 2002 **12235**
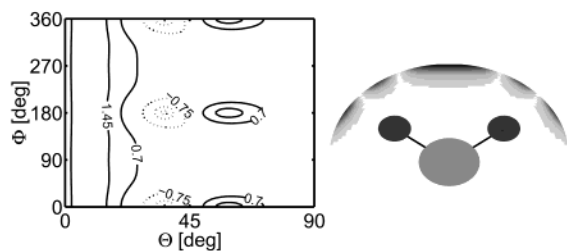
Figure 9. Angular dependence of the probability density of the sixth excited state (040) of A_1 symmetry of the Cl⁻···H₂O complex with four nodes in the θ coordinate (librationally excited).

the stretching mode. For example, the spacings between the states forming the in-plane bending librational progression reduce to 250 and 200 cm^{-1} in the deuterated complex. In some cases (e.g., state 040), the librationally excited states even fall in energy below those that do not possess librational but only stretching excitation. Thus, the ordering of states in the deuterated complex differs from that of the hydrogenated analogue.

4.2. Neutral Complex. Similarly to the anionic complex, stationary states on the three low-lying electronic potentials of the neutral system have been explored using the imaginary time propagation technique. Resulting energy level diagrams are presented in Figure 10. The neutral complex is much more weakly bound compared to the anionic one, its ground state (see Figure 10a) having a stabilization energy of 964 cm^{-1} (note that the dissociation threshold of the electronic ground state equals -294 cm^{-1}). The corresponding wave function, depicted in Figure 11a, reflects the difference in the character of the intermolecular interaction between the anionic and neutral cases.[23,25] Unlike in the anionic complex (see Figure 7), the angular probability density of the chlorine in the neutral ground state has a maximum near the water oxygen (compare also with the optimal geometries in Figure 2). The wave function is substantially more delocalized than the anionic one, indicating large amplitude librational motion of the two hydrogen atoms. The radial probability density peaks at $R = 2.8$ Å, which is the optimal chlorine−water distance in the neutral complex.

The upper two electronic potential energy surfaces are almost purely repulsive with a shallow minimum that supports only a few bound states. The ground vibrational state of the first excited electronic state is stabilized by 106 cm^{-1} and that of the second excited electronic state by 218 cm^{-1}. The angular character of the wave functions corresponding to both of these states is similar to that of the ground state (see Figure 11a), the radial probability density peaking at a somewhat larger chlorine−water separation, $R = 3.7$ Å for the first and $R = 3.6$ Å for the second excited electronic state.

Rather than presenting a detailed analysis of the wave functions corresponding to all of the energy levels given in Figure 10, we focus on selected states of A_1 symmetry to illustrate the characteristic properties of the system under study. First of all, the validity of the picture of separable modes (intermolecular stretching mode, in-plane water bend, and out-of-plane water bend) is rather questionable for the neutral complex. The angular character of the wave functions resembles that of a hindered rotor rather than a water molecule librating around an equilibrium geometry. Because of this behavior, as well as mixing of the radial and the two angular modes, straightforward assignment of quantum numbers in the sense of single mode excitations is not possible. For the ground electronic potential surface, the first excited state within the A_1 manifold can be identified as the fundamental excitation of the
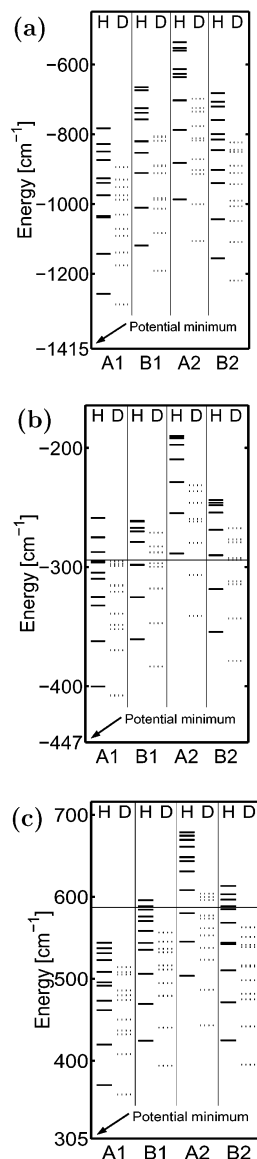
Figure 10. Energy level diagram of low-lying rovibrational states of (a) ground and (b, c) lowest two electronically excited states of neutral Cl•···H₂O (left subcolumns) and Cl•···D₂O (right subcolumns) complexes for all irreducible representations of the C_{2v} point group. Horizontal lines correspond to the dissociation thresholds after inclusion of the spin−orbit interaction (-294 cm^{-1} for the ground and first excited states and 588 cm^{-1} for the second excited state). Energy levels above these horizontal lines represent quasibound resonances.

intermolecular stretching vibration (115 cm^{-1}). Second and third excited states are both of a mixed character, exhibiting radial, as well as librational/rotational, excitation (Figure 11b), while the fourth excited state (Figure 11c) shows a purely rotational excitation. Although in general separability breaks down, analysis of the radial and angular probability densities in the way illustrated by Figure 11 can provide information about the prevailing character of a given state, as well as about the degree of the radial−angular nonseparability. Similar analysis has been performed also for the low-lying rovibrational states on the first electronically excited potential surface and is reported in section 5.2 in connection with the interpretation of the photoelectron spectra.

As mentioned above, the two electronically excited potential surfaces are rather shallow, supporting only several bound states. Therefore, using the imaginary time propagation method (see section 3.2), we have been able to calculate also quasi-bound
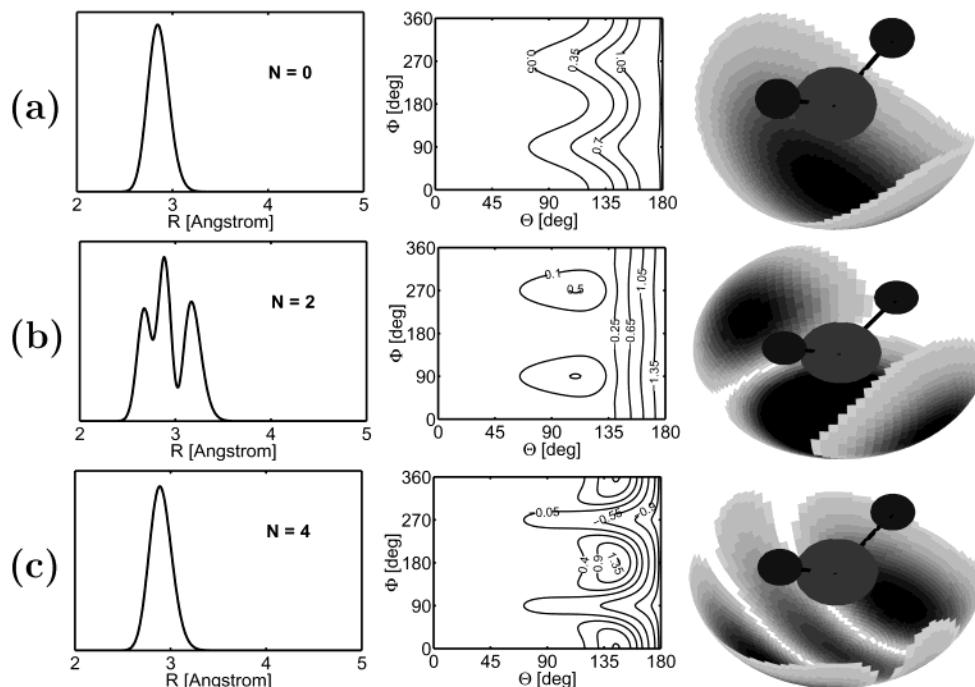
Figure 11. Wave functions of selected low-lying bound rovibrational states of the neutral Cl$^{\bullet}$···H$_2$O complex: (a) ground state; (b) second excited state; (c) fourth excited state of A_1 symmetry.

resonant states for these two potentials. Apparently, these resonances are sufficiently long-lived that a method essentially tailored for bound-states calculations can retrieve them. In Figure 10b,c, these are the states lying above the vertical line depicting the dissociation threshold.

In analogy to the anionic complex, deuteration makes a significant difference also in the neutral system. It influences predominantly the angular degrees of freedom by affecting the reduced masses of bending modes or, in other words, the rotational constants. Therefore, in the case of the hindered water rotation in the neutral complex, the effect of deuteration on the corresponding energy levels is even more dramatic than that in the anion, because the ratio between the rotational constants (and hence the rotational energies) of D$_2$O and H$_2$O is almost 1:2. At the same time, deuteration has less effect on zero-point energy because in the limit of a free rotor there is no ZPE and also because the chlorine−water binding in the neutral complex is weaker than that in the anionic one. Thus, the reduction of the total ZPE (ΔZPE = 30 cm^{-1}) is smaller in the neutral compared to the anion, and a shift of the origin of the photoelectron spectrum toward higher energies is predicted upon deuteration.

5. Results: Real-Time Propagation

5.1. Dynamics upon Electron Photodetachment. The initial wave packets, that is, the wave functions of the two lowest vibrational states of the anionic system, one of A_1 symmetry and the other of B_1 symmetry (the tunneling pair), were propagated independently on the three low-lying electronically adiabatic potential energy surfaces of the neutral system, for both Cl$^{\bullet}$···H$_2$O and Cl$^{\bullet}$···D$_2$O cases.

The resulting autocorrelation function (ACF) corresponding to propagation on the electronic ground state of the Cl$^{\bullet}$···H$_2$O complex is presented in Figure 12. The upper panel shows both A_1 and B_1 autocorrelation functions, which after initial decay remain almost constant during the whole propagation (18 ps), indicating that long-lived states of the neutral system are
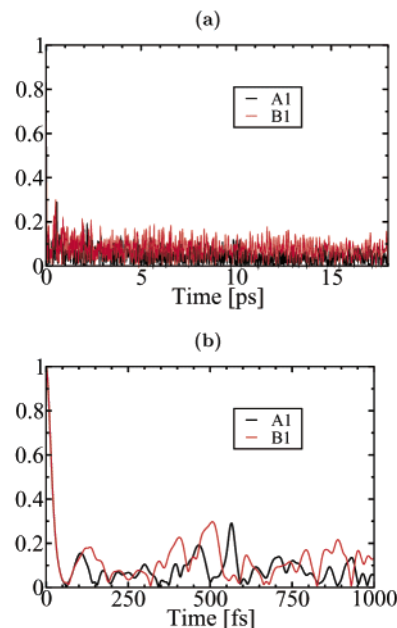
Figure 12. Autocorrelation functions obtained by propagating the A_1 (black line) and B_1 (red line) initial wave packets on the ground electronic PES of the neutral Cl$^{\bullet}$···H$_2$O complex. Panel a shows the total propagation time of 18 ps; panel b displays in more detail the first 1000 fs of the propagation.

populated upon electron photodetachment from its anionic precursor. The initial decay can be rationalized by comparing the ground adiabatic PES of the neutral complex (Figure 5) and the initial wave packet (Figure 7). The maximum amplitude of both A_1 and B_1 wave functions ($R = 3.15$ Å, $\theta = 44°$, and $\phi = 0°$) practically coincides with the geometry, where the PES of the neutral complex has a maximum in the angular coordinates. If the anionic wave packet was classically localized at its maximum, vertical promotion onto the ground PES of the neutral cluster would place it above the dissociation threshold. Therefore, there is only a low propensity of the wave packet to revisit
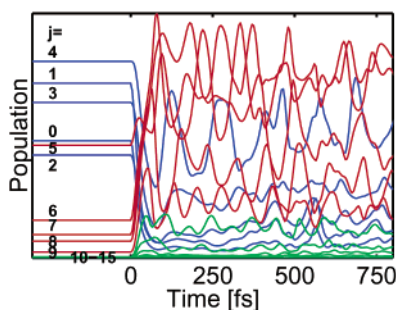
Figure 13. Time evolution of populations $P(j,t)$ defined by eq 12. The populations are divided into three groups by the amount of rotational excitation involved: $j = 0-4$ (blue); $j = 5-9$ (red); $j = 10-15$ (green). At time $t = 0$, the populations correspond to the anionic ground state (the initial wave function).

the initial Franck–Condon region during the propagation. Interestingly, the oscillations of the B_1 ACF have a somewhat larger amplitude compared to the A_1 ACF, indicating that the spectral features will be more intense in the former case.

In the lower panel of Figure 12, the ACFs in the first 1000 fs after electron photodetachment are shown in more detail. For both symmetries, the ACF initially decays to zero very fast, in about 60 fs, which is followed by the first recurrence at 110–130 fs. On the basis of our previous classical simulations,[25] as well as the reasoning given below, it is possible to assign these features of the early dynamics to internal water rotation that is excited upon electron photodetachment: Before the heavy atoms move away significantly from their initial positions, rotation of the water molecule brings the hydrogens back to the vicinity of the Franck–Condon region, thus causing a partial revival in the ACF. Because water molecule is an asymmetric rotor with a complex rotational pattern, the ACF signal becomes irregular very early. Nevertheless, another rather large recurrence can be identified in the region of 500–600 fs, corresponding to one period of the intermolecular stretching vibration (see below).

A useful piece of information shedding light onto the photodetachment dynamics can be extracted from the time dependence of populations of the individual rotational states, $|jk\rangle = Y_{jk}^{(S)}(\theta,\phi)$. This is illustrated in Figure 13, in which we present the time evolution of populations

$$P(j,t) = \sum_{\substack{k=0 \\ (k\ even)}}^{j} \int |\chi_{j,k}^{(A_1)}(R,t)|^2\ dR \qquad (11)$$

of the states of A_1 symmetry. In the above expression, we have integrated over the radial coordinate and summed all of the individual contributions from distinct values of projection quantum number k for fixed angular momentum j. In Figure 13, individual lines correspond to distinct values of j ranging from 0 to 15, which exhausts the size of the angular basis used for propagation. A time interval of the first 750 fs following the photodetachment is shown. We have divided the populations somewhat arbitrarily into three groups with respect to the amount of rotational excitation involved: states with low rotation, $j = 0-4$ (blue color), moderate rotation, $j = 5-9$ (red color), and high rotation, $j = 10-15$ (green color). At the beginning, the populations match the stationary distribution of the anionic ground state (initial condition), where the most populated states are those with low rotational excitation. After photodetachment, the situation changes dramatically, as the population of the low-rotation states decreases in intensity, while the moderate-rotation states become the most populated ones. Also some of the high-
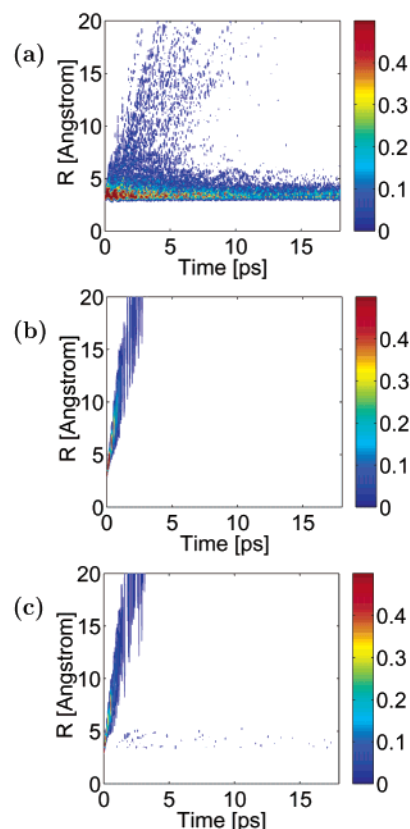
Figure 14. Time evolution of radial probability density (corresponding to chlorine–water distance) on (a) ground, (b) first excited, and (c) second excited electronic potential energy surfaces of the neutral Cl$^\bullet$···H$_2$O complex.

rotation states increase in amplitude slightly; however, there is virtually no excitation of the highest rotational states considered ($j_{max} = 15$), indicating that the size of the angular basis is sufficient for the description of the process. The above-described increase of the average angular momentum that follows the electron photodetachment can be explained in terms of excitation of the internal water rotation, from the zero-point librational motions of the hydrogen atoms in the anionic initial state to the fast rotation of the water molecule, hindered to a certain extent by the interaction with the chlorine atom in the nascent neutral system. Qualitatively, such behavior has been observed already in our previous classical dynamics study,[25] which revealed that, despite the fact that the system upon electron photodetachment is placed above the dissociation threshold, most of the excess energy is deposited very rapidly into the internal water rotation, stabilizing thus the complex against direct dissociation.

Time evolution of the chlorine–water distance supports this picture. In Figure 14a, a contour plot of the radial probability density $\rho(R;t)$ (for time-independent definition, see eq 10) as a function of intermolecular distance R and time t is depicted. A substantial part of the wave function remains confined to the region between 3 and 4.5 Å (corresponding to a bound complex) during the whole propagation with only little direct dissociation and some more delayed dissociation, mostly within the first 10 ps. Several intermolecular vibrations can be identified right after photodetachment. The period of the vibrations is about 500 fs, a value similar to that obtained from the classical propagation.[25] Analogous plots for the upper two adiabatic electronic surfaces are shown in Figure 14b,c. Unlike the case of the ground-state potential, there is hardly any indication of bound complexes
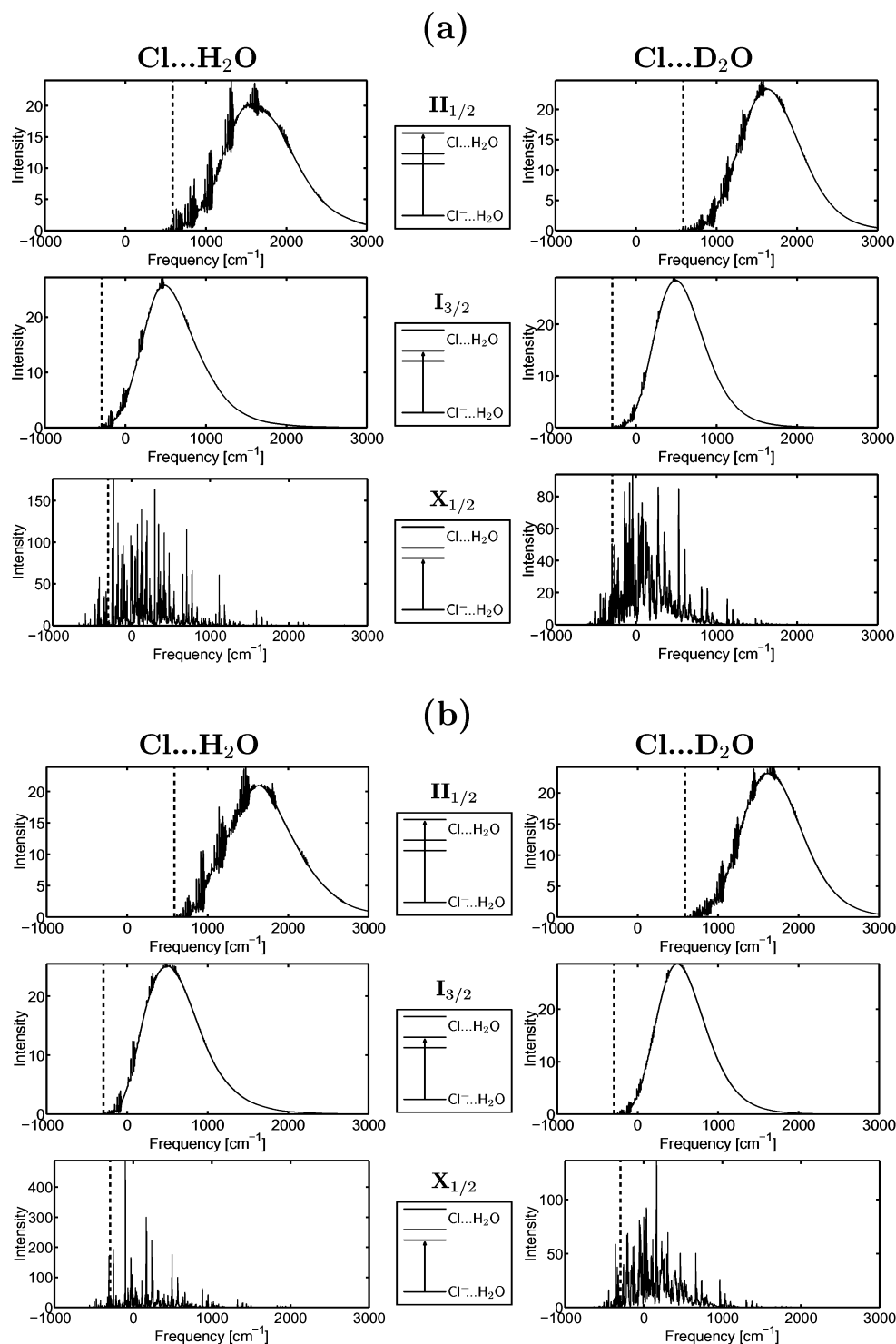
Figure 15. Electron photodetachment spectra of $Cl^-\cdots H_2O$ and $Cl^-\cdots D_2O$ complexes obtained by propagating (a) the A_1 and (b) the B_1 initial wave function on each of the lowest three electronic states of the neutral complex. The dashed lines depict the dissociation thresholds after inclusion of the spin−orbit interaction (-294 cm^{-1} for the ground and first excited states and 588 cm^{-1} for the second excited state). Spectral features to the right of the dashed lines are due to direct dissociation and resonances.

being created upon photodetachment into the upper two electronic states. On the contrary, the time evolution of the radial probability density on these two states corresponds almost entirely to direct dissociation.

5.2. Photoelectron Spectra. The very different dynamical behavior of the neutral complex in the ground electronic state, as compared to the first two electronically excited ones, is clearly reflected in the simulated spectra obtained by propagating both the A_1 (Figure 15a) and B_1 (Figure 15b) initial wave functions

independently on each of the lowest three electronic potential energy surfaces of the $Cl^\bullet\cdots H_2O$ and $Cl^\bullet\cdots D_2O$ complexes. The frequency scale is identical for all of the three neutral electronic states; thus, the three spectra will overlap in the actual experiment. Zero on the frequency axis corresponds to the dissociation energy of the neutral complex into Cl and H_2O fragments without the inclusion of the spin−orbit interaction. The dissociation energies of the three electronic states after addition of the spin−orbit term ($-^1/_3\Delta = -294$ cm^{-1} and $^2/_3\Delta$
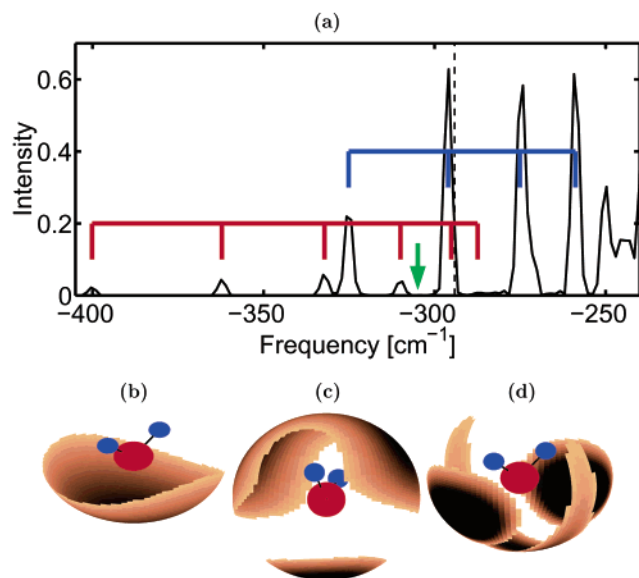
Figure 16. (a) Enlarged section of the low-energy region of the A_1 spectrum of the first electronically excited state of Cl•···H₂O complex with two vibrational progressions, one (marked in red) corresponding to the ground and the other (marked in blue) to the first excited rotational state of the water molecule. Angular plots of the ground and first excited rotational wave functions are depicted in panels b and c. An example of a state that has a negligible Franck−Condon overlap with the initial wave function and, therefore, does not appear in the spectrum (see the green arrow) is shown in panel d.

$= 588$ cm^{-1} with $\Delta = 882.4$ cm^{-1} being the spin−orbit constant of the chlorine atom) are denoted by dashed lines. To the left of the respective dissociation thresholds, each of the spectra contains weak signals coming from the bound states (including the ground states on the corresponding potentials); however, most of the signal is due to dissociation and resonances. The dissociative character of the underlying dynamics is most apparent in the spectra arising from the transitions to the mostly repulsive first and second excited electronic states. They are dominated by broad envelopes of fwhm in the range of 800−900 cm^{-1}, corresponding to direct departure from the Franck−Condon region (with no return) in 6−7 fs, with sharp resonances superimposed on top of them. Similar arguments apply also to the ground-state spectrum of the Cl•···H₂O complex in which, however, the substantially different character of the potential energy surface leads to population of a large number of intense resonances that mask the underlying broad envelope. In the ground-state spectrum of the Cl•···D₂O complex, the dissociative envelope is more pronounced because of a smaller ratio between the intensity of the resonances and the height of the envelope (note the difference in intensity scales for different spectra).

The structure of the spectra consists of bands that can be interpreted both in terms of the aforementioned dynamical arguments and in terms of the bound-state analysis (see Section 4.2) as bands corresponding to individual rotational states of water molecule that are populated after the dynamics is initiated by the electron photodetachment. In the low-energy range of the spectra, particularly in the case of the ground state, the bands are overlapping, and thus, it is difficult to see this feature directly. However, with the help of the analysis of the bound-state wave functions, the validity of the above interpretation can be proved. As an example, we focus on the low-energy region of the spectrum corresponding to the first electronically excited state of Cl•···H₂O complex (see Figure 16). Figure 16a shows several bound states supported by the shallow potential (to the left of the dashed line marking the dissociation threshold).
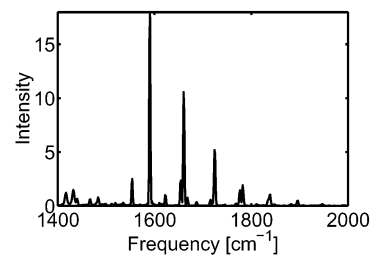
Figure 17. Enlarged section of the high-energy region of the A_1 spectrum of the ground electronic state of Cl•···H₂O complex showing one rotational band with anharmonic vibrational progression.

Note that the finite width of these peaks is due to the limited length of propagation, which determines the frequency resolution of our computer experiment. To the right of the dashed line, the onset of the broad dissociative envelope with sharp peaks due to long-lived resonances is shown. Analysis of the wave functions of the stationary states of A_1 symmetry (see Figure 10b) that correspond to the peaks in the spectrum depicted in Figure 16a revealed two vibrational progressions, one (marked in red) related to the ground state of the internal (hindered) water rotation (see Figure 16b) and the other (marked in blue) to the first rotationally excited state of A_1 symmetry (see Figure 16c). The spacing between vibrational lines is 38, 30, 22, and 15 cm^{-1} in the former progression and 29, 21, and 16 cm^{-1} in the latter. These anharmonic vibrational progressions corresponding to a single rotational state reflect slower vibrational motion of the halogen atom with respect to the rotating water molecule. The difference in overall intensities between the two above-mentioned vibrational progressions can be rationalized by comparing the overlaps of the two rotational wave functions depicted in Figure 16b,c with the initial anionic wave function (see Figure 7). The Franck−Condon overlap of the ground rotational state wave function with the anionic one is clearly smaller than that in the rotationally excited case. An example of a state with an extremely low-intensity peak in the spectrum (denoted by a green arrow) due to an almost vanishing overlap with the initial wave function is given in Figure 16d, which depicts the angular probability density of the second rotationally excited state within the A_1 manifold.

In the high-energy range of the spectra, individual bands of resonances are well separated with increasing spacing between the bands typical for rotational lines. The spacing between the first two peaks of the anharmonic vibrational progression superimposed on a single rotational band, which corresponds to the intermolecular stretching vibration in an effective chlorine−(rotating) water potential, is about 70 cm^{-1} in the ground-state spectrum of the Cl•···H₂O complex (see Figure 17). This in the time domain corresponds to roughly 500 fs, that is, the intermolecular stretching vibration period already encountered in Figure 14. Vibrational progressions in the spectra of the upper two electronic states are more dense with the fundamental spacing of 31 cm^{-1} for the first excited PES and 34 cm^{-1} for the second excited PES. It reflects the fact that these two potentials are more shallow in the stretching coordinate compared to the ground electronic state. The lifetime of these resonances is typically higher than the length of simulation (which has been adopted to match the experimental resolution).

The comparison of the Cl•···H₂O and Cl•···D₂O spectra enables us to discuss the effects of deuteration on the dynamics following the electron photodetachment from the respective anionic precursors. The heavier D₂O responds less readily to the initial torque than the lighter H₂O molecule, and therefore, the wave packet leaves the Franck−Condon region more slowly

in the deuterated case. This is manifested in the spectrum (see Figure 15) as the decrease in the width of the broad envelope upon deuteration. Consequently, a smaller part of the excess energy is initially deposited into the (nondissociative) internal water rotation in the $Cl^- \cdots D_2O$ complex compared to the $Cl^{\bullet} \cdots H_2O$ one, while more energy goes from the very beginning into the (dissociative) intermolecular stretching vibration. Thus, the resonances are much less intense in the spectra of the deuterated system, and the $Cl^{\bullet} \cdots D_2O$ complex dissociates faster than the $Cl^{\bullet} \cdots H_2O$ one. As mentioned previously in section 4.1, vibrational progressions corresponding to the chlorine–water stretching motion remain practically unchanged by deuteration. The opposite is true for water rotation in which the dramatic reduction of the rotational constants leads to the rotational bands being more densely spaced in the deuterated case compared to the hydrogenated one. The spectra of the deuterated system are thus more compact. In addition, the spectral origins are blue-shifted (e.g., by 107 cm^{-1} in the ground electronic state).

Although experimental ZEKE spectra of the $Cl^- \cdots H_2O$ complex have not yet been published, we can compare our simulated spectra to measured spectra of a similar complex, in which chlorine is substituted by iodine.[20,45] The plausibility of comparison of the experimental $I^- \cdots H_2O$ and the simulated $Cl^- \cdots H_2O$ photoelectron spectra is based on the fact that one can expect a qualitatively similar character of the intermolecular potential, which is in both cases determined mainly by the properties of the half-filled valence p-orbital of the halogen atom. The difference in the reduced masses is small because both halogens are rather heavy compared to the water molecule, and it is mainly the latter one that moves. The main difference represents a much higher asymptotic splitting of the neutral states of the iodine–water complex as compared to its chlorine–water counterpart because the spin–orbit constant of iodine is about 10 times larger than that of chlorine.

Spectra for both the iodine–water complex and its fully deuterated analogue have been measured recently.[20,45] In the case of the ground state spectrum of the deuterated complex, a pattern resembling a vibrational progression can be clearly identified with the spacing between the first two lines about 60 cm^{-1},[45] which corresponds very well to our simulated spectrum. The experimental spectrum arising from the $II_{1/2}$ state exhibits an analogous vibrational progression, only with smaller spacing of about 30 cm^{-1}. The uppermost potential is thus more shallow than the ground PES, an observation that is consistent with the simulated results. The simulated spectra extend over much larger interval of frequencies (about 4000 cm^{-1} for each PES) than the measured spectra. Because of the unfavorable signal-to-noise ratio, frequency windows of only about 400 cm^{-1} corresponding to the width of a single rotational band with a vibrational progression superimposed on it are accessible for each spin–orbit component in the experiment. Because of these experimental limitations, the computer simulation is in this particular case capable of providing a more detailed insight into the photodetachment dynamics.

6. Summary

The photoelectron spectra of $Cl^- \cdots H_2O$ and $Cl^- \cdots D_2O$ clusters have been modeled by means of quantum dynamical simulations on the three low-lying electronic surfaces of the neutral complexes including explicitly all three intermolecular nuclear degrees of freedom. Using both the time-dependent quantum approach and imaginary time propagation for evaluation of stationary states of the anionic and neutral systems, we have been also able to quantitatively interpret the spectra in

terms of the underlying quantum dynamics. The dynamics is driven by the large differences between the shapes of the anionic and neutral intermolecular potential energy surfaces. Upon electron photodetachment, the neutral complex is born primarily above the dissociation threshold. At the lowest neutral potential, most of the excess energy is initially deposited into the hindered rotation of the water molecule; therefore, the cluster does not significantly dissociate directly, but rather long-lived resonances occur. The situation is reversed for the two upper neutral surfaces, in which direct dissociation dominates. The observed resonances form bands, each corresponding to a particular internal rotational state of water, with vibrational structure reflecting progressions in the intermolecular stretch. Analogous vibrational progressions have been directly observed in the ZEKE experiment for the $I^- \cdots H_2O$ complex.

References and Notes

(1) Muller-Dethlefs, K.; Schlag, E. W. *Annu. Rev. Phys. Chem.* **1991**, *42*, 109.

(2) Waller, I. M.; Kitsopoulos, T. N.; Neumark, D. M. *J. Chem. Phys.* **1990**, *94*, 2240.

(3) Gantefor, G.; Cox, D. M.; Kaldor, A. *J. Chem. Phys.* **1990**, *94*, 854.

(4) Drechsler, G.; Baessmann, C.; Boesl, U.; Schlag, E. W. *J. Mol. Spectrosc.* **1995**, *348*, 337.

(5) Herzberg, G. *Molecular Spectra and Molecular Structure I*; Krieger Publishing Company: Malabar, FL, 1989.

(6) Schatz, G. C.; Ratner, M. A. *Quantum Mechanics in Chemistry*; Prentice Hall: Englewood Cliffs, NJ, 1993.

(7) Heller, E. J. *J. Phys. Chem.* **1978**, *68*, 2006.

(8) Heller, E. J. *Acc. Chem. Res.* **1981**, *14*, 368.

(9) Markovich, G.; Giniger, R.; Levin, M.; Cheshnovsky, O. *J. Chem. Phys.* **1991**, *95*, 9416.

(10) Combariza, J. E.; Kestner, N. R.; Jortner, J. *Chem. Phys. Lett.* **1993**, *203*, 423.

(11) Combariza, J. E.; Kestner, N. R.; Jortner, J. *J. Chem. Phys.* **1993**, *100*, 2851.

(12) Xantheas, S. S. *J. Phys. Chem.* **1996**, *100*, 9703.

(13) Chaban, G. M.; Jung, J. O.; Gerber, R. B. *J. Phys. Chem. A* **2000**, *104*, 2772.

(14) Roszak, S.; Koval, M.; Gora, R. W.; Leszczynski, J. *J. Chem. Phys.* **2001**, *115*, 3469.

(15) Perera, L.; Berkowitz, M. J. *J. Chem. Phys.* **1991**, *95*, 1954.

(16) Perera, L.; Berkowitz, M. J. *J. Chem. Phys.* **1992**, *96*, 8288.

(17) Perera, L.; Berkowitz, M. J. *J. Chem. Phys.* **1994**, *100*, 3085.

(18) Yeh, I. C.; Perera, L.; Berkowitz, M. J. *Chem. Phys. Lett.* **1997**, *264*, 423.

(19) Schenter, G. K.; Garrett, B. C.; Voth, G. A. *J. Chem. Phys.* **2000**, *113*, 5171.

(20) Bässmann, C.; Boesl, U.; Yang, D.; Drechsler, G.; Schlag, E. W. *Int. J. Mass. Spectrom.* **1996**, *159*, 153.

(21) Zhao, Y.; Yourshaw, I.; Reiser, G.; Arnold, C. C.; Neumark, D. M. *J. Chem. Phys.* **1994**, *101*, 6538.

(22) Yourshaw, I.; Zhao, Y.; Neumark, D. M. *J. Chem. Phys.* **1994**, *105*, 351.

(23) Roeselova, M.; Jacoby, G.; Kaldor, U.; Jungwirth, P. *Chem. Phys. Lett.* **1998**, *293*, 309.

(24) Jungwirth, P.; Roeselova, M.; Gerber, R. B. *J. Chem. Phys.* **1999**, *110*, 9833.

(25) Roeselova, M.; Kaldor, U.; Jungwirth, P. *J. Phys. Chem. A* **2000**, *104*, 6523.

(26) Aquilanti, V.; Liuti, G.; Pirani, F.; Vecchiocattivi, F. *J. Chem. Soc., Faraday Trans.* **1989**, *85*, 955.

(27) Becker, C. H.; Cassavecchia, P.; Lee, Y. T. *J. Chem. Phys.* **1979**, *70*, 5477.

(28) Ellison, F. O. *J. Am. Chem. Soc.* **1963**, *85*, 3540.

(29) Hutson, J. *J. Chem. Phys.* **1990**, *92*, 157.

(30) Bacic, Z.; Miller, R. E. *J. Phys. Chem.* **1996**, *100*, 12945.

(31) Pople, J. A.; Head-Gordon, M.; Raghavachari, K. *J. Chem. Phys.* **1987**, *87*, 5968.

(32) Kendall, R. A.; Dunning, T. H., Jr.; Harrison, R. J. *J. Chem. Phys.* **1992**, *96*, 6796.

(33) Woon, D. E.; Dunning, T. H., Jr. *J. Chem. Phys.* **1993**, *98*, 1358.

(34) Frisch, M. J.; Trucks, G. W.; Schlegel, H. B.; Scuseria, G. E.; Robb, M. A.; Cheeseman, J. R.; Zakrzewski, V. G.; Montgomery, J. A., Jr.; Stratmann, R. E.; Burant, J. C.; Dapprich, S.; Millam, J. M.; Daniels, A. D.; Kudin, K. N.; Strain, M. C.; Farkas, O.; Tomasi, J.; Barone, V.; Cossi, M.; Cammi, R.; Mennucci, B.; Pomelli, C.; Adamo, C.; Clifford, S.; Ochterski, J.; Petersson, G. A.; Ayala, P. Y.; Cui, Q.; Morokuma, K.; Malick, D. K.; Rabuck, A. D.; Raghavachari, K.; Foresman, J. B.; Cioslowski, J.; Ortiz, J. V.; Stefanov, B. B.; Liu, G.; Liashenko, A.; Piskorz, P.; Komaromi, I.; Gomperts, R.; Martin, R. L.; Fox, D. J.; Keith, T.; Al-Laham, M. A.; Peng, C. Y.; Nanayakkara, A.; Gonzalez, C.; Challacombe, M.; Gill, P. M. W.; Johnson, B. G.; Chen, W.; Wong, M. W.; Andres, J. L.; Head-Gordon, M.; Replogle, E. S.; Pople, J. A. *Gaussian 98*; Gaussian, Inc.: Pittsburgh, PA, 1998.

(35) Choi, J.-H.; Kuwata, K. T.; Cao, Y.-B.; Okumura, M. *J. Phys. Chem. A* **1998**, *102*, 503.

(36) Ayotte, P.; Weddle, G. H.; Johnson, M. A. *J. Chem. Phys.* **1999**, *110*, 7129.

(37) Schinke, R. *Photodissociation Dynamics*; Cambridge University Press: Cambridge, U.K., 1993.

(38) Kroto, H. W. *Molecular rotation spectra*; Wiley: New York, 1975.

(39) Cotton, F. A. *Chemical Applications of Group Theory*; Interscience Publishers, John Wiley and Sons: New York−London−Sydney, 1967.

(40) Press, W. H.; Teukolsky, S. A.; Vetterling, W. T. *Numerical Recipes in Fortran*; Cambridge University Press: Cambridge, U.K., 1992.

(41) Kosloff, R. *Annu. Rev. Phys. Chem.* **1984**, *45*, 145.

(42) Tal-Ezer, H.; Kosloff, R. *J. Chem. Phys.* **1984**, *89*, 3967.

(43) Kosloff, R. *J. Phys. Chem.* **1988**, *92*, 2087.

(44) Zdanska, P.; Nachtigallova, D.; Nachtigall, P.; Jungwirth, P. *J. Chem. Phys.* **2001**, *114*, 5974.

(45) Boesl, U. et al. Unpublished results.